# Decomposition reactions for NaAlH4, Na3AlH6, and NaH: First-principles study

AUTHOR(S):

Ke, XZ; Tanaka, I

CITATION:

Ke, XZ ...[et al]. Decomposition reactions for NaAlH4, Na3AlH6, and NaH: First-principles study. PHYSICAL REVIEW B 2005, 71(2): 024117.

ISSUE DATE:

2005-01

URL:

http://hdl.handle.net/2433/39867

PHYSICAL REVIEW B **71**, 024117 (2005)

# Decomposition reactions for $NaAlH_4$, $Na_3AlH_6$, and NaH: First-principles study

Xuezhi Ke[1,*] and Isao Tanaka[2,†]
[1]*Fukui Institute for Fundamental Chemistry, Kyoto University, Kyoto 606-8103, Japan*
[2]*Department of Materials Science and Engineering, Kyoto University, Sakyo, Kyoto 606-8501, Japan*
(Received 15 July 2004; revised manuscript received 12 October 2004; published 31 January 2005)

The electronic properties and lattice dynamics of the sodium alanate phases have been studied by the density functional calculations. The phases include $NaAlH_4$ (space group, $I4_1/a$), $Na_3AlH_6$ (space group, $P2_1/n$), and NaH (space group, $Fm$-$3m$). The electronic properties are discussed on the basis of the electronic band structures, the atomic charges, the bond overlap population analysis, and the Born effective charges. The phonon dispersion relations and phonon density of states (DOS) of the phases are calculated by a direct force-constant method. Within the quasiharmonic approximation, the calculated thermodynamic functions including the heat capacity, the vibrational enthalpy, and the vibrational entropy are in good agreement with experimental values. Three decomposition reactions are studied based on the thermodynamic functions. The reactions are (1) $NaAlH_4 \rightarrow \frac{1}{3}Na_3AlH_6 + \frac{2}{3}Al + H_2$, (2) $\frac{1}{3}Na_3AlH_6 \rightarrow NaH + \frac{1}{3}Al + \frac{1}{2}H_2$, and (3) $NaH \rightarrow Na + \frac{1}{2}H_2$. The reactions (1), (2), and (3) are predicted to take place at 285, 390, and 726 K, respectively, which are in good agreement with the experiment (353, 423, and 698 K, respectively). The individual contributions to the reactions including the enthalpy and entropy are investigated. We found that the enthalpy for the reaction is almost constant, and the net entropy contribution ($T\Delta S$) to the reaction is approximately equal to the entropy contribution of the $H_2$ gas molecule (produced in that reaction).

DOI: 10.1103/PhysRevB.71.024117 PACS number(s): 63.20.−e, 71.15.Mb, 64.60.−i, 65.40.−b

## I. INTRODUCTION

Hydrogen is the fuel for the proton exchange membrane fuel cells. The operating temperature for this fuel cell is below 100 °C.[1] To meet the requirement of the fuel cell and also from the practical point of view, hydrogen should be stored under the desired condition such as at the room temperature and at (or around) the standard pressure of 1 atm. For the applications of hydrogen in the vehicles, the development of the compact, light and affordable containment is necessary. So far, there are very limited materials that can achieve these goals. The complex sodium alanate of $NaAlH_4$ is a promising candidate since the hydrogen storage in this hydride is reversible under the moderate temperature and pressure (with the help of catalyst).[2] H is released from the alanate via the following two steps:

$$NaAlH_4 \overset{3.7\ \text{wt. \%}}{\Rightarrow} \frac{1}{3}Na_3AlH_6 + \frac{2}{3}Al + H_2, \quad (1)$$

$$\frac{1}{3}Na_3AlH_6 \overset{1.9\ \text{wt. \%}}{\Rightarrow} NaH + \frac{1}{3}Al + \frac{1}{2}H_2, \quad (2)$$

where the first reaction releases 3.7 wt. % hydrogen and the second reaction releases 1.9 wt. % hydrogen. Thus this material has a total theoretical capacity of 5.6 wt. % hydrogen, which is above the target (5 wt. %) of the International Energy Agency.

The alanate of $NaAlH_4$ has received considerable attention since the recent work by Bogdanović and Schwickardi, who demonstrated that the catalyst could enhance the performance of the alanate significantly.[2] Currently, this alanate is being considered as a promising candidate for the application of the onboard vehicles because of its high hydrogen weight capacity and low cost.[7] Experimentally, there is a lot of work about this alanate[2–9] (only the references related to our discussion are listed here). However, the theoretical work about this alanate is still limited. The geometric and electronic structures of $NaAlH_4$ were studied from the first principles.[10–13] To our knowledge, the lattice dynamics and thermodynamic functions of the sodium alanate are rarely studied theoretically. Very recently, the thermodynamics of the lithium alanates was studied by a first-principles method.[14] In that paper the reaction enthalpies of $LiAlH_4$ and $Li_3AlH_6$ at 298 K were calculated.

Of particular interest in this paper is to understand the lattice dynamics of the sodium alanate phases. The phases include $NaAlH_4$, $Na_3AlH_6$, and NaH. The vibrational properties such as the phonon dispersion relations and phonon density of states (DOS) will be calculated based on a direct force-constant method. Based on the integrated phonon DOS, the thermodynamic functions will be derived within the quasiharmonic approximation (QHA). The functions include the heat capacity, the vibrational enthalpy and entropy, and the free energy. Further, these thermodynamic functions will be used to study the decomposition reactions in Eqs. (1) and (2). We think that the obtained information is useful for us to get a better understanding of the vibrational properties and the thermodynamic behavior in these phases. In addition, the electronic properties of the phases will be discussed based on the electronic structures.

The remainder of this paper is organized in three sections. In Sec. II, the theoretical methods are introduced. Mainly, two methods are used here. One is the density functional method for the total energy and force-matrix calculations, another is the direct force-constant method for phonon calculations. In Secs. III A–III D, the results are presented and discussed. Section III A is the geometric and electronic structures, and Born effective charge tensors of the alanate phases. Section III B is the phonon dispersion relations and phonon density of states of the phases. Section III C is the

 

TABLE I. Calculated dielectric constants for $NaAlH_4$, $Na_3AlH_6$, and NaH along three directions of the polarization. Dielectric constant $\varepsilon$ for each material is obtained from the average of these three directions, i.e., $\varepsilon=\frac{1}{3}(\varepsilon_{100}+\varepsilon_{010}+\varepsilon_{001})$. Here, 100, 010, and 001 represent the polarized directions in $x$, $y$, and $z$, respectively. For NaH, the dielectric constants in three directions are the same (isotropic), i.e., $\varepsilon_{100}=\varepsilon_{010}=\varepsilon_{001}$. For $NaAlH_4$, $\varepsilon_{100}=\varepsilon_{010}$ $(\approx\varepsilon_{001})$. For $Na_3AlH_6$, $\varepsilon_{100}\approx\varepsilon_{010}\approx\varepsilon_{001}$.

| | $\varepsilon_{100}$ | $\varepsilon_{010}$ | $\varepsilon_{001}$ | $\varepsilon$ |
|---|---|---|---|---|
| $NaAlH_4$ | 3.22 | 3.22 | 3.28 | 3.24 |
| $Na_3AlH_6$ | 3.11 | 3.10 | 3.13 | 3.11 |
| NaH | 3.09 | 3.09 | 3.09 | 3.09 |

thermodynamic functions of the phases. Section III D is the decomposition reactions in Eqs. (1) and (2). In Sec. IV, the concluding remarks are made.

## II. THEORETICAL METHODS

The calculations were performed using the plane wave basis VASP code,[15,16] implementing the generalized gradient approximation (GGA) of Perdew and Wang.[17] The interaction between the ion and the electron is described by the projector augmented wave method (PAW)[18,19] with plane waves up to a cutoff energy of 400 eV. The configurations Al $3s^23p^1$, Na $2p^63s^1$, and H $1s^1$ are treated as the valence electrons. For the lattice dynamics calculations, we need to do more than 1000 single point calculations for the large supercells. In order to speed up the calculations, only Na $3s^1$ was treated as a valence electron. We found that the energy difference between these two cases is negligible, for an example of $NaAlH_4$, the vibrational zero-point energy difference is only 0.1 meV per atom between the configurations of the Na $2p^63s^1$ and Na $3s^1$. Brillouin-zone integrations were performed on the grid of Monkhost-Pack procedure.[20] For medium size cells ($4.95\times4.95\times10.98$ Å$^3$ for $NaAlH_4$, and $5.35\times5.35\times7.71$ Å$^3$ for $Na_3AlH_6$), $5\times5\times2$ and $4\times4\times3$ $k$-point meshes were used for $NaAlH_4$ and $Na_3AlH_6$, respectively. The total energy convergences for both cases within 0.2 meV per atom were achieved (compared with the more dense meshes of $7\times7\times3$ and $5\times5\times4$ for $NaAlH_4$ and $Na_3AlH_6$, respectively). For a large supercell ($\sim10$ Å $\times\sim10$ Å $\times\sim10$ Å), a $2\times2\times2$ $k$-point mesh was used. The total energy convergence within 0.05 meV per atom was achieved (compared with a $4\times4\times4$ $k$-point mesh).

To calculate the phonon dispersion and phonon density of states, we use a direct *ab into* force-constant approach, which was implemented by Parlinski.[21] In this method a specific atom is displaced to induce the forces to act on the surrounding atoms, which are calculated via the Hellmann-Feynman theorem. The forces are collected to form the force-constant matrices and dynamical matrices. The dynamical matrices are solved by the direct method based on the harmonic approximation.[21] In order to avoid the interaction between the two images of the displaced atom (due to the periodical boundary condition), it is very necessary to use a relatively large supercell for the calculations of the force matrices. We try to use the supercell in such a way that it is closest to a spherical shape. The supercells contain 96 and 80 atoms for $NaAlH_4$ and $Na_3AlH_6$, respectively.

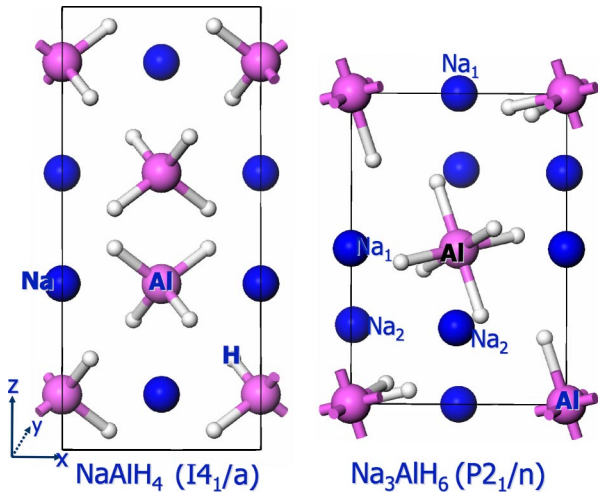


FIG. 1. Crystal structures of $NaAlH_4$ (right) and $Na_3AlH_6$ (left). The biggest ball represents aluminum atom, the smaller black ball is sodium atom, and the smallest ball is H atom. The space groups for $NaAlH_4$ and $Na_3AlH_6$ are $I4_1/a$ and $P2_1/n$, respectively. Wyckoff coordinates for $NaAlH_4$ are Al (0,0.25,0.125), Na (0,0.25,0.625), and H (0.235,0.391,0.044). Wyckoff coordinates for $Na_3AlH_6$ are Al (0,0,0), $Na_1$ (0.5,0,0.5), $Na_2$ (0.243,−0.045,−0.2465), $H_1$ (0.317,−0.049,0.215), $H_2$ (0.225,0.172,−0.044), and $H_3$ (−0.097,0.265,0.065).

As will be discussed in the later section, the lattices of $NaAlH_4$, $Na_3AlH_6$, and NaH belong to the ionic (polar) crystals. For the polar crystals the infrared optical modes at the Γ point are normally split into the longitudinal optical (LO) modes and transversal optical (TO) modes (so-called LO/TO splitting) due to the long-range Coulomb interaction (caused by the displacement of atoms). As pointed out by Kunc and Martin,[22] the LO/TO splitting at the Γ point cannot be directly calculated by the direct approach, and only the TO mode is obtained without further approximation. One solution is to use an elongated supercell to recover this mode. However, this is unrealistic for the current system because the elongated cells are beyond our computational capability (particularly for $NaAlH_4$ and $Na_3AlH_6$). Alternatively, a nonanalytical dynamical matrix can be taken into account approximately. The following matrix is responsible for the LO/TO splitting:

$$\Delta D_{ij,\alpha\beta}(\mathbf{q}\to0)=\frac{4\pi e^2}{\varepsilon V\sqrt{M_iM_j}}\frac{(\mathbf{q}\cdot\mathbf{Z}_i^*)_\alpha(\mathbf{q}\cdot\mathbf{Z}_j^*)_\beta}{|\mathbf{q}|^2}, \quad (3)$$

where $\mathbf{q}$ is the wave vector, $\varepsilon$ is the optical macroscopic dielectric function, $V$ is the volume of the primitive unit cell, $M_i$ and $\mathbf{Z}_i^*$ are the mass and the Born effective charge tensor for the $i$th atom, respectively, and $\alpha$ and $\beta$ are the Cartesian indices. In our calculations, the value of $\varepsilon$ is obtained from the average of three lattice directions (there are almost isotropic for the current lattices), i.e., $\varepsilon=\frac{1}{3}(\varepsilon_{100}+\varepsilon_{010}+\varepsilon_{001})$. In practice, the imaginary part of the dielectric constant is ob-

TABLE II. Comparison between the calculated and measured lattice parameters for $NaAlH_4$, $Na_3AlH_6$, and NaH. The second column is also the calculated results, in which the zero-point (ZP) energies of the lattices are considered. The lattices are expanded a bit due to the ZP motions.

| Parameters | Calculated (Å) | Calculated (Å)[a] | Measured (Å) |
|---|---|---|---|
| | $NaAlH_4$ (space group $I4_1/a$) | | |
| $a$ | 4.979 | 5.044 | 5.027[b] |
| $c$ | 11.103 | 11.330 | 11.371 |
| | $Na_3AlH_6$ (space group $P2_1/n$) | | |
| $a$ | 5.349 | 5.416 | 5.454[b] |
| $b$ | 5.533 | 5.606 | 5.547 |
| $c$ | 7.707 | 7.833 | 7.811 |
| $\beta$ | 89.86 | 89.80 | 89.83 |
| | NaH (space group $Fm$-$3m$) | | |
| $a$ | 4.820 | 4.887 | 4.882[c] |

[a]Calculated results including the zero-point energy of the lattices.
[b]Experiment in Ref. 6, where the temperature is above room temperature.
[c]Experiment in Ref. 27, the value is derived from the density of 1.37 g/cm$^3$.

tained from the electronic structure, using the joint density of states between the valence and conduction bands and the optical matrix overlap.[23] From the Kramers-Kronig relations, the real part of the dielectric constant can be obtained. Since the imaginary part is related to the band gap, and the real band gaps for these materials are unknown (DFT usually underestimates the gap), the band-gap corrections (also called scissor operator) are not applied in our calculations. The calculated dielectric constants for $NaAlH_4$, $Na_3AlH_6$, and NaH are compiled in Table I. The Born effective charges are obtained from the Berry phase calculations. This matrix only affects the LO modes at the Γ point. More discussion about this term can be found in the references.[21,24–26]

## III. RESULTS AND DISCUSSION

### A. Geometric and electronic structures, and Born effective charge tensors

In this section, the geometric and electronic structures, and the Born effective charges for $NaAlH_4$, $Na_3AlH_6$, and NaH will be presented. For clarity, this section is split into two sections I and II. Section III A 1 is about the geometric and electronic structures, and Sec. III A 2 is about the Born effective charge tensors.

#### *1. Geometric and electronic structures*

The geometric structures of $NaAlH_4$ and $Na_3AlH_6$ are shown in Fig. 1, where the lattice parameters are compiled in Table II. It shows that the calculated results agree well with the experimental data. When the zero-point energies are included, Table II shows the lattices are expanded a bit, which refines the results a bit. The lattice of NaH (space group, $Fm$-$3m$) is a face-centered-cubic (fcc) structure, which is the

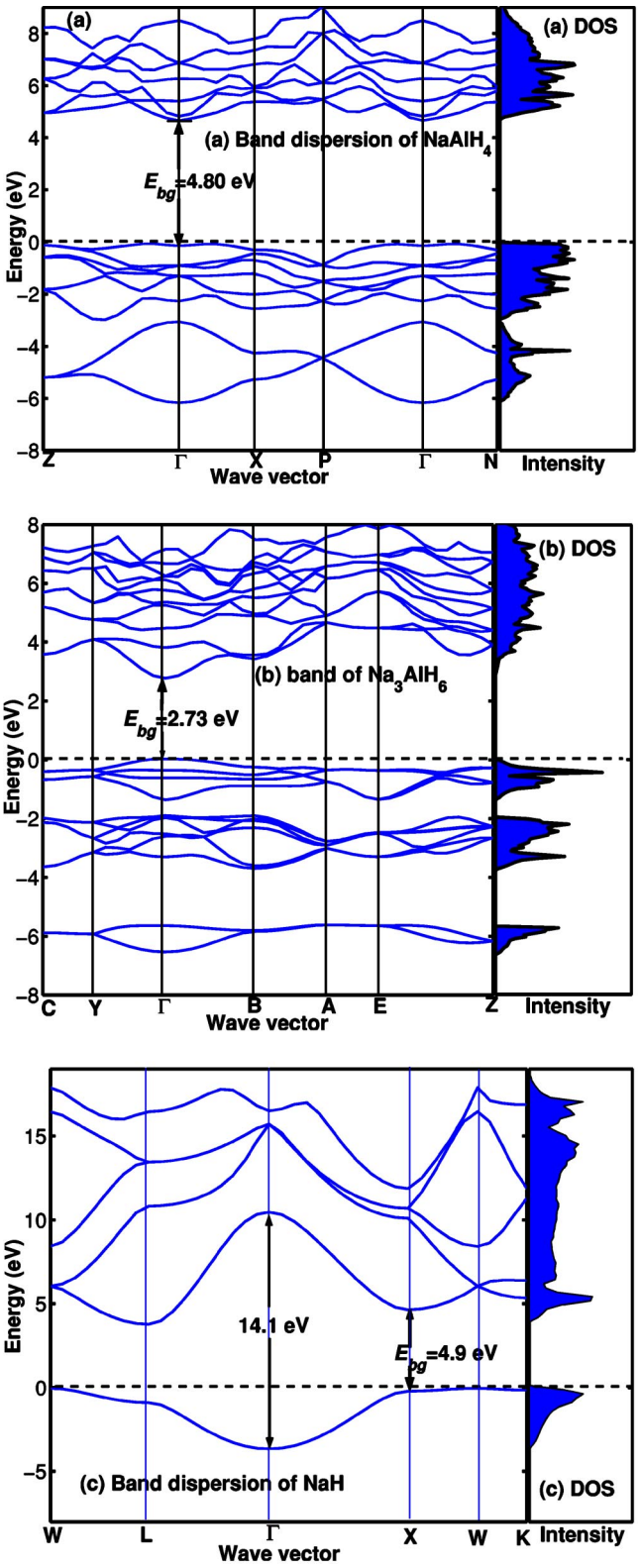


FIG. 2. Electronic band structures and total density of states (DOS) for $NaAlH_4$ (a), $Na_3AlH_6$ (b), and NaH (c) along some high symmetry directions in the first Brillouin zone. The symbol of $E_{bg}$ denotes the direct band gap. The energies below −8 eV are omitted in the figures.

TABLE III. Calculated total charges and ionic charges of the atoms in $NaAlH_4$, $Na_3AlH_6$, and NaH.

| Elements | Total charge ($e$) | Ionic charge (electric) ($e$) |
|---|---|---|
| | $NaAlH_4$ (space group $I4_1/a$) | |
| H | 1.49 | −0.49 |
| Al | 2.50 | 0.50 |
| Na | 5.55 | 1.45 |
| | $Na_3AlH_6$ (space group $P2_1/n$) | |
| $H_1$ | 1.50 | −0.50 |
| $H_2$ | 1.51 | −0.51 |
| Al | 2.91 | 0.09 |
| $Na_1$ | 6.29 | 0.71 |
| $Na_2$ | 5.90 | 1.10 |
| | NaH (space group $Fm$-3$m$) | |
| H | 1.51 | −0.51 |
| Na | 6.49 | 0.51 |

same as that of NaCl (hydrogen replacing chlorine).

The electronic structures discussed here include the electronic band structures, the total charges, and the bond overlap population analysis.

The calculated band structures and the corresponding electronic density of states (DOS) for $NaAlH_4$, $Na_3AlH_6$, and NaH are presented in Figs. 2(a)–2(c), respectively. For $NaAlH_4$, the current band dispersion relations and the total DOS are similar to other calculations.[10,11] For NaH, the current band dispersion relations are similar to those of the related lattice of LiH.[28] For $Na_3AlH_6$, its band dispersion relations are somewhat similar to those of $NaAlH_4$, e.g., the minimum direct band gaps for both lattices are located at the Γ point, and the dispersion relations at the highest occupied states (more or less at the lowest unoccupied states) are similar for both lattices. This indicates that the lattices of $NaAlH_4$ and $Na_3AlH_6$ belong to the same class of crystals. The direct band gaps are denoted as the $E_{bg}$ in the figures. Note that the real band gaps may be larger than these values due to the well-known underestimation by the density functional theory. The band gaps for $NaAlH_4$, $Na_3AlH_6$, and NaH are 4.8, 2.7, and 4.9 eV, respectively, indicating these lattices are strongly ionic crystals.

To get a better understanding of the electronic properties in the lattices, we have calculated the atomic charges and the bond overlap population values based on the Mulliken charge analysis.[29,30,32] It should be noted that the absolute values of the atomic charges based on the Mulliken analysis cannot be uniquely defined, since they are very sensitive to the atomic basis set.[31] However, the consideration of these relative values (as well as the magnitudes) can provide us useful information.[32] The calculated charges for the atoms in $NaAlH_4$, $Na_3AlH_6$, and NaH are compiled in Table III. It shows that the total charge of a H atom in these lattices is greater than 1.0 electron. In other words, H looks like an anion. This situation is similar to that of H in metals, where the H atom always accepts electrons from metals.[33,34] While this is different from that of H in oxides, where the H donates electrons to oxygen ion. However, this does not mean these lattices are metals. Actually, the partial DOS shows that the H band in the lattices is very different from that of H in metals. For H in these lattices, the whole valence bands are strongly dominated by the H atom, and the intensity of the H band is close to that of the sodium valence band (not plotted here, see Ref. 11). While for H in metals (except alkali metals), the main position of the H band usually is below the valence band of the host metals (relative to the Fermi level). Notice that the calculated electric charges for Na atoms in $NaAlH_4$ and $Na_3AlH_6$ are greater than the nominal ionic charges of +1. This may be an artifact by the Mulliken population analysis in the current study. We can rely on these values only relatively.

The bond overlap population (BOP) can provide useful information about the bonding property between atoms. A high BOP value indicates a strong covalent bond, while a low BOP value indicates an ionic interaction. The calculated BOP values for the lattices are compiled in Table IV. It shows that all of the H—Al bonds are highly covalent, and the covalent H—Al bonds in $NaAlH_4$ are stronger than those in $Na_3AlH_6$. The BOP values for the H—Na bonds are small, indicating that these are ionic bonds. It can be seen from the table that the interactions between the two H atoms are quite weak.

### *2. Born effective charge tensors*

For the ionic crystal, as mentioned in the methodological section that the Coulomb interaction affects the LO/TO splittings at the Γ point. This interaction is directly related to the Born effective charge tensors, e.g., a finite dipole moment of $\mathbf{p}$ is created by the displacement ($\Delta\mathbf{u}$) of the $i$th atom,

$$\mathbf{p} = Z^*_{i,\alpha,\beta} \times \Delta\mathbf{u}, \tag{4}$$

where $Z^*_{i,\alpha,\beta}$ is the Born effective charge tensor, and $\Delta\mathbf{u}$ is the displacement of the $i$th atom in the unit cell. According to the polarization theory,[35,36] the total difference in polarization

TABLE IV. Calculated bond overlap population values between the two atoms in $NaAlH_4$, $Na_3AlH_6$, and NaH.

| Bond | Bond length(Å) | Bond order population |
|---|---|---|
| | $NaAlH_4$ (space group $I4_1/a$) | |
| H—Al | 1.631 | 0.88 |
| H—Na | 2.395–2.404 | −0.10–−0.08 |
| H—H | 2.631–2.882[a] | −0.07–−0.02 |
| | $Na_3AlH_6$ (space group $P2_1/n$) | |
| H—Al | 1.764 | 0.64 |
| H—Al | 1.776 | 0.65 |
| H—Al | 1.784 | 0.62 |
| H—Na | 2.283 | −0.02 |
| H—Na | 2.299–2.307 | 0.07–0.21 |
| H—H | 2.488–2.531 | −0.10–−0.09 |
| | NaH (space group $Fm$-3$m$) | |
| H—Na | 2.410 | 0.39 |
| H—H | 3.409 | −0.05 |

[a]Within or between the two tetrahedrons of $AlH_4$.

TABLE V. Calculated Born effective charges for NaH, $NaAlH_4$, and $Na_3AlH_6$. The space groups for NaH, $NaAlH_4$, and $Na_3AlH_6$ are $Fm$-3$m$, $I4_1/a$, and $P2_1/n$, respectively.

| | Position[a] | $Z^*_{xx}$ | $Z^*_{yy}$ | $Z^*_{zz}$ | $Z^*_{xy}$ | $Z^*_{xz}$ | $Z^*_{yx}$ | $Z^*_{yz}$ | $Z^*_{zx}$ | $Z^*_{zy}$ |
|---|---|---|---|---|---|---|---|---|---|---|
| | | | | | NaH | | | | | |
| Na | | 0.96 | 0.96 | 0.96 | 0 | 0 | 0 | 0 | 0 | 0 |
| H | | −0.96 | −0.96 | −0.96 | 0 | 0 | 0 | 0 | 0 | 0 |
| | | | | | $NaAlH_4$ | | | | | |
| Al | 4$a$ | 1.64 | 1.64 | 2.01 | 0 | 0 | 0 | 0 | 0 | 0 |
| Na | 4$b$ | 1.20 | 1.20 | 1.09 | 0 | 0 | 0 | 0 | 0 | 0 |
| H | 16$f$ | −0.74 | −0.68 | −0.78 | −0.06 | 0.07 | −0.06 | 0.12 | 0.07 | 0.12 |
| | | | | | $Na_3AlH_6$ | | | | | |
| Al | 2$a$ | 2.04 | 2.08 | 2.04 | −0.01 | −0.05 | −0.01 | 0.02 | 0.03 | 0.08 |
| $Na_1$ | 2$d$ | 1.05 | 1.06 | 1.05 | 0 | 0.08 | 0.05 | −0.03 | −0.05 | 0.03 |
| $Na_2$ | 4$e$ | 1.05 | 1.04 | 1.07 | 0.04 | −0.01 | 0.01 | 0.05 | 0.02 | 0.05 |
| $H_1$ | 4$e$ | −1.03 | −0.70 | −0.87 | 0.06 | −0.23 | 0.05 | 0.07 | −0.24 | 0.03 |
| $H_2$ | 4$e$ | −0.89 | −0.84 | −0.88 | −0.14 | 0.16 | −0.13 | 0.18 | 0.17 | 0.15 |
| $H_3$ | 4$e$ | −0.69 | −1.07 | −0.87 | 0.09 | 0.06 | 0.08 | −0.22 | 0.07 | −0.22 |

[a]Wyckoff position. For Wyckoff coordinates, please see the caption of Fig. 1.

between the distorted and undistorted structures is

$$\Delta\mathbf{P} = \Delta\mathbf{P_e} + \Delta\mathbf{P_{ion}}, \tag{5}$$

where $\Delta\mathbf{P_e}$ is the electronic contribution obtained from the Berry-phase polarization approach,[36] and $\Delta\mathbf{P_{ion}}$ is the ionic contribution by

$$\Delta\mathbf{P_{ion}} = \frac{|e|z_i\Delta\mathbf{u}}{V}, \tag{6}$$

where $z_i$ is the valence atomic number of the $i$th atom, $V$ is the volume of the unit cell, and $\Delta\mathbf{u}$ is the displacement of the $i$th atom in the unit cell. Once $\Delta\mathbf{P}$ is known, the Born effective charge tensor for the $\beta$ component can be obtained from the formula,

$$Z^*_{i,\alpha,\beta} = \frac{V}{|e|}\frac{(\Delta\mathbf{P})_\alpha}{\Delta\mathbf{u}}, \tag{7}$$

where $\alpha$ denotes the direction of the polarization. In the Berry-phase calculations, we chose the displacement of 0.05 Å, and used a set of strings of 6-**k** points (parallel to some chosen reciprocal lattice vectors) to calculate the electronic polarization. With these settings we found the results are well converged.

The calculated Born effective charge tensors for NaH, $NaAlH_4$, and $Na_3AlH_6$ are compiled in Table V. For NaH, the Born effective charge tensors are isotropic and diagonal due to the high symmetry of $Fm$-3$m$, i.e., $Z^*_{ij}=Z^*\delta_{ij}$ for each atom. For $NaAlH_4$ (with $I4_1/a$ symmetry), there are three nonequivalent atoms in the unit cell including Al, Na, and H atoms. For Al and Na atoms, the effective charges are diagonal in the Cartesian frame with $Z^*_{xx}=Z^*_{yy}\neq Z^*_{zz}$. For H in $NaAlH_4$, the effective charge is off-diagonal, and there are some symmetry operations in some planes, e.g., $Z^*_{xy}=Z^*_{yx}$, $Z^*_{xz}=Z^*_{zx}$, and $Z^*_{yz}=Z^*_{zy}$. For $Na_3AlH_6$ ($P2_1/n$, can be considered as a monoclinic cell), there are six nonequivalent atoms in the unit cell, which are labelled as Al, $Na_1$, $Na_2$, $H_1$, $H_2$, and $H_3$ in the table. The Born effective charge tensors for these elements are off-diagonal due to the low symmetry. As a whole, the magnitudes of the effective charges in $Na_3AlH_6$ are close to those in $NaAlH_4$.

It can be seen from Table V that the dynamics charges for these lattices are close to the nominal ionic charges (+1 for Na and −1 for H) except for Al. For Al, its dynamics charges are 1.64–2.08, which are smaller than the nominal charge of +3. These indicate that the LO/TO splittings at the Γ point may be not very pronounced.[26] For NaH, the situation is different and there is a large LO/TO splitting as will be discussed later.

### B. Phonon dispersion relations and phonon density of states

For $NaAlH_4$, the calculated phonon dispersion relations along several lines of high symmetry in the first Brillouin zone are presented in Fig. 3. As discussed in the preceding section that $NaAlH_4$ belongs to an ionic crystal, therefore the LO/TO splittings at the Γ point should occur. This phenomena are found and denoted as the small arrows in Fig. 3. Since there are 12 atoms in the primitive cell, there are three acoustic modes and thirty-three optical modes, which are shown in Fig. 3.

The frequencies at the Γ point in Fig. 3 are summarized in Table VI. According to the symmetry analysis (crystal point group: $C_{4h}$), the optical modes at the Γ point can be classified into the following symmetry species:

$$\Gamma_{\text{opt}} = 3A_g(R) + 4A_u(I) + 5B_g(R) + 5E_g(R) + 4E_u(I) + 3B_u, \tag{8}$$

where the notations of $R$ and $I$ mean Raman active mode and infrared active mode, respectively. The mode of $B_u$ is a Raman- and infrared-inactive silent mode. Among these modes, $E_g(R)$ and $E_u(I)$ are doubly degenerate (perpendicular

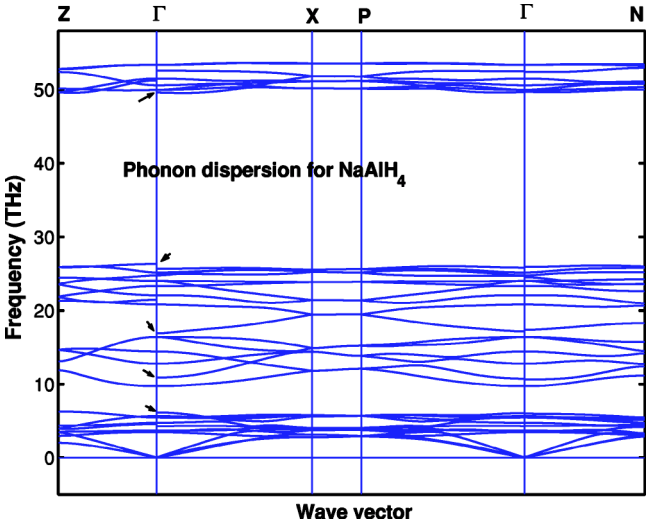


FIG. 3. Calculated phonon dispersion curves for $NaAlH_4$ (space group, $I4_1/a$) along several lines of high symmetry in the first Brillouin zone. The arrows show the LO/TO splittings.

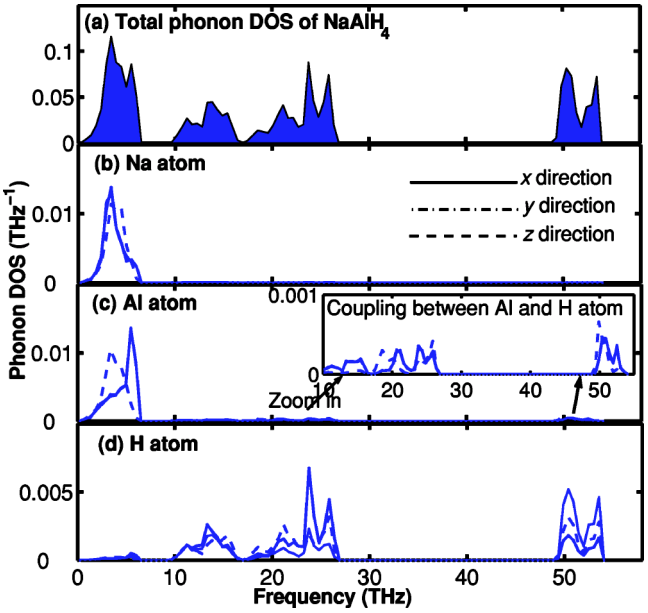


FIG. 4. Calculated total and partial phonon density of states (DOS) in $NaAlH_4$. (a) is the total phonon DOS, and (b), (c), and (d) are the partial phonon DOS for Na, Al, and H atoms, respectively. The partial DOS is plotted along three directions of the $x$, $y$, and $z$. For Na and Al atoms, the phonon DOS long the $x$ and $y$ directions are identical (degenerate).

to the $z$ direction). When assigning the experimental Raman values to these species, we have noticed that a few modes in the experiment are missing, e.g., the calculated results in Table VI show that the values of $E_g(4)$ and $B_g(4)$ are 5.439 THz and 5.633 THz, respectively. However, only one peak of 5.216 THz was observed in the experiment.[8] The reason for the absence is not clear. Probably, the peaks of these modes are too weak to be observed or they were not activated under the conditions of the experiment (such as the temperature of 25 °C). In this particular case, we assign one experimental value to two calculated modes (the two values are close to each other), which are indicated as the asterisks in Table VI. Table VI shows that the calculated Raman frequencies are in good agreement with the experimental values within 5% error, which is typical when the direct method is used.

The total and partial phonon DOS for $NaAlH_4$ are presented in Fig. 4, in which Fig. 4(a) is the total phonon DOS, and Figs. 4(b)–4(d) are the partial phonon DOS for the Na,

TABLE VI. Frequency modes at the Γ point of the Brillouin zone for $NaAlH_4$. The units are in THz.

| Modes | Calculated | Measured[a] | Modes | Calculated | Measured[a] | Modes | Calculated | Measured[a] |
|---|---|---|---|---|---|---|---|---|
| Raman | | | | | | | | |
| $E_g(1)$ | 49.956 | 50.365* | $B_g(1)$ | 51.484 | 50.356* | $A_g(1)$ | 53.333 | 53.033 |
| $E_g(2)$ | 24.004 | 24.343 | $B_g(2)$ | 25.135 | 25.392 | $A_g(2)$ | 22.046 | 22.934* |
| $E_g(3)$ | 16.389 | 15.319 | $B_g(3)$ | 23.303 | 22.934* | $A_g(3)$ | 12.752 | 12.561 |
| $E_g(4)$ | 5.439 | 5.216* | $B_g(4)$ | 5.633 | 5.216* | | | |
| $E_g(5)$ | 3.457 | 3.208 | $B_g(5)$ | 3.658 | 3.478 | | | |
| Infrared | | | | | | | | |
| $E_u(1)$ | 50.582(TO) | | $Au_g(1)$ | 49.596(TO) | | | | |
| | 51.483(LO) | | | 51.225(LO) | | | | |
| $E_u(2)$ | 20.791(TO) | | $Au_g(2)$ | 25.640(TO) | | | | |
| | 22.046(LO) | | | 26.285(LO) | | | | |
| $E_u(3)$ | 9.692(TO) | | $Au_g(3)$ | 16.871(TO) | | | | |
| | 10.875(TO) | | | 21.440(LO) | | | | |
| $E_u(4)$ | 4.730(TO) | | $Au_g(4)$ | 4.268(TO) | | | | |
| | 6.115(TO) | | | 4.575(LO) | | | | |
| Silent | | | | | | | | |
| $B_u(1)$ | 53.344 | | $B_u(2)$ | 24.764 | | $B_u(3)$ | 14.409 | |

[a]Raman data from Ref. 8.

Al, and H atoms, respectively. The partial phonon DOS is plotted along three directions of the *x*, *y*, and *z*. For Na and Al atoms, the vibrational modes along the *x* and *y* directions are identical, and the modes along the *z* are slightly different from those of the *x* and *y* directions. Since the mass of H atom is much smaller than that of Na or Al atom, Fig. 4 shows that the high frequency modes (above 10 THz) are dominated by H atom, and the low frequency modes (below 10 THz) are dominated by Na and Al atoms. The figure shows that the partial phonon DOS between Na and Al atoms does not differ much because the mass of Na atom is close to that of Al atom. One obvious difference between Na and Al atoms is that only Al atom gives the high frequency modes with the frequencies between 48 and 54 THz (see the inset in Fig. 4). The examination of these frequencies (for Al atom) reveals that the vibrations are composed of the antisymmetric and symmetric stretching modes of the H—Al bonds. Qualitatively, this can be understood in terms of the bond overlap population. The bond overlap population analysis shows that the H—Al bond is highly covalent and the H—Na bond is ionic. Therefore it is natural that only the vibrations between the H and Al atoms are coupled. As a result, Al atom also participates in the high frequency modes.

For $Na_3AlH_6$, the calculated total and partial phonon DOS are presented in Fig. 5, in which Fig. 5(a) is the total phonon DOS, and Fig. 5(b)–5(d) are the partial phonon DOS for Na, Al, and H atoms, respectively. The partial phonon DOS also is plotted along three directions of the *x*, *y*, and *z*. For Na and Al atom, the vibrational modes along the directions of the *x*, *y*, and *z* are almost identical although their intensities are slightly different. For H atom, the vibrational modes are anisotropic due to the low symmetry. Due to the same reason as the $NaAlH_4$, the high frequency modes in $Na_3AlH_6$ are dominated by H atom, and the low frequency modes are dominated by Na and Al atoms. Comparison of the H frequency modes between the $NaAlH_4$ and $Na_3AlH_6$ shows that there are some obvious differences. For H vibrations in $NaAlH_4$, the frequency modes are separated by a big gap from 26.8 to 48.9 THz [see Fig. 4(d)]. While for H vibrations in $Na_3AlH_6$, there is not such a big gap [see Fig. 5(d)]. On the other hand, the high frequency modes above the gap (in $NaAlH_4$) are from 48.9 to 54.1 THz, which are greater than the highest frequency (45.8 THz) in $Na_3AlH_6$. All of the high frequencies are found to be composed of the stretching modes of the H—Al bonds. Again, the differences can be understood qualitatively in terms of the bond overlap population. The bond overlap population analysis shows that the covalent H—Al bond in $NaAlH_4$ is stronger than that in $Na_3AlH_6$. Therefore the potential energy wells (PEW) for H vibrations in $NaAlH_4$ are steeper than those for H vibrations in $Na_3AlH_6$, and consequently the high frequency modes in $NaAlH_4$ are shifted to the higher modes. As a result, the frequency gap is created. This steeper PEW also is the reason that the frequency modes above the gap in $NaAlH_4$ are greater than the highest frequency in $Na_3AlH_6$.

For NaH, the calculated phonon dispersion relations and the corresponding phonon DOS are presented in Fig. 6. The dotted line represents the results without considering the Born effective charges. It can be seen from the figure that there is a giant LO/TO splitting at the Γ point between the

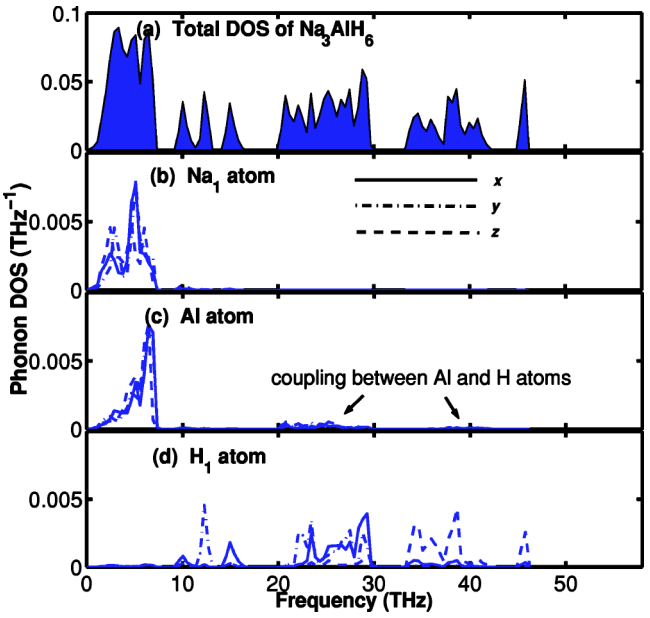


FIG. 5. Calculated total and partial phonon density of states (DOS) of $Na_3AlH_6$. (a) is the total phonon DOS, and (b), (c), and (d) are the partial phonon DOS for $Na_1$, Al, and $H_1$ atoms, respectively. For $Na_2$, its frequency region is the same as that for $Na_1$, and the difference between the $Na_1$ and $Na_2$ is that they have different intensities. This is also true for the $H_1$, $H_2$, and $H_3$. The partial DOS is plotted along three directions of the *x*, *y*, and *z*.

$T_{1u}$(TO) and $T_{1u}$(LO) modes. This is different from those of $NaAlH_4$ and $Na_3AlH_6$, where the splittings are not significant. The phonon DOS shows that the highest frequency for H vibrations in NaH is 26.7 THz, which is much smaller than that for H vibrations in $NaAlH_4$ (54.1 THz) or $Na_3AlH_6$ (45.8 THz). Again, these differences can be understood qualitatively in terms of the bond overlap population. As discussed in this section the H—Al bond is highly covalent and the H—Na bond is ionic. Therefore the potential energy wells (PEW) for H vibrations in NaH should be much shallower than those for H vibrations in $NaAlH_4$ and $Na_3AlH_6$ (in the stretching modes of the H—Al bonds), and consequently the frequency modes in NaH are much lower than those in $NaAlH_4$ and $Na_3AlH_6$. Due to this shallower PEW, H atom in NaH can displace a longer distance than that in $NaAlH_4$ or $Na_3AlH_6$. According to Eq. (4), a larger displacement ($\Delta\mathbf{u}$) will cause a larger dipole moment (Born effective charges for H atom in these lattices are almost the same, see Table V). The larger forces in NaH are parallel to the displacement. As a result, the giant LO/TO splitting at the Γ point is created in NaH. Due to the ionic (weak) interaction between the H and Na atoms in NaH, there is almost no vibrational coupling between the two atoms. As a result, the high frequency modes of H atom are almost completely separated from the low frequency modes of Na atom.

### C. Thermodynamic functions

The thermodynamic functions include the heat capacity ($C_v$ and $C_p$), the vibrational entropy ($S_{(T)}$), the internal en-

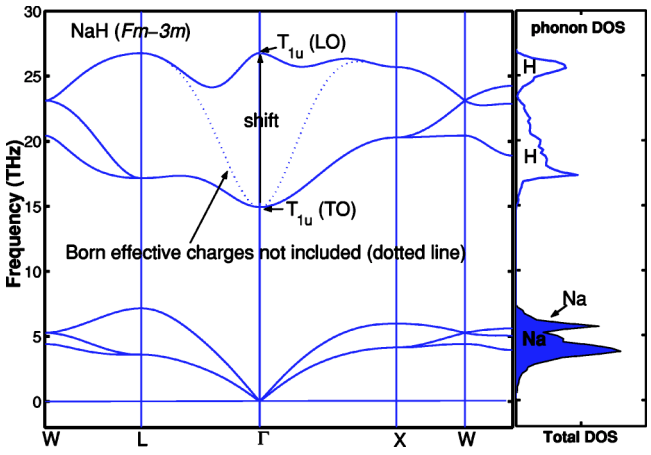


FIG. 6. Calculated phonon dispersion relations and phonon density of states (DOS) for NaH (space group $Fm$-3$m$). The dispersions are along some high symmetry directions in the first Brillouin zone. The dotted line represents the results without considering the Born effective charges. The frequencies of the $T_{1u}$(TO) and $T_{1u}$(LO) (infrared optical modes) are 14.938 and 26.749 THz, respectively. The right-hand side is the total phonon DOS.

ergy ($E_{(T)}$) and the free energy. The heat capacity of $C_v$ at the constant volume is calculated by

$$C_v = rk_B \int_0^\infty d\omega g(\omega) \left(\frac{\hbar\omega}{k_B T}\right)^2 \frac{\exp\left(\frac{\hbar\omega}{k_B T}\right)}{\left[\exp\left(\frac{\hbar\omega}{k_B T}\right) - 1\right]^2}, \quad (9)$$

where $g(\omega)$ is the phonon DOS of the unit cell, $r$ is the number of degrees of freedom in the unit cell, $\hbar$ is the Planck constant, $k_B$ is the Boltzmann constant, and $T$ is the temperature. The low temperature limit of $C_v$ is

$$\lim_{T\to 0} C_v = 0. \quad (10)$$

Within the harmonic phonons the heat capacity at the constant volume ($C_v$) and at the constant pressure ($C_p$) are equal. In our calculations, the lattice expansion is taken into account, therefore the $C_p$ can be approximately estimated by

$$C_p = C_v + \alpha^2 VBT, \quad (11)$$

where $\alpha$ is the thermal expansivity $[=(1/V)(\partial V/\partial T)]$, $V$ is the volume, and $B$ is the bulk modulus of the system. According to the third law of thermodynamics, the entropy of a perfect lattice at the $T=0$ is equal to zero. The vibrational entropy at elevated temperature is described by

$$S_{(T)} = rk_B \int_0^\infty g(\omega) \left\{ \left(\frac{\hbar\omega}{2k_B T}\right) \left[\coth\left(\frac{\hbar\omega}{2k_B T}\right) - 1\right] - \ln\left[1 - \exp\left(\frac{-\hbar\omega}{k_B T}\right)\right] \right\} d\omega. \quad (12)$$

The internal energy of the unit cell including the zero-point (ZP) energy is calculated by

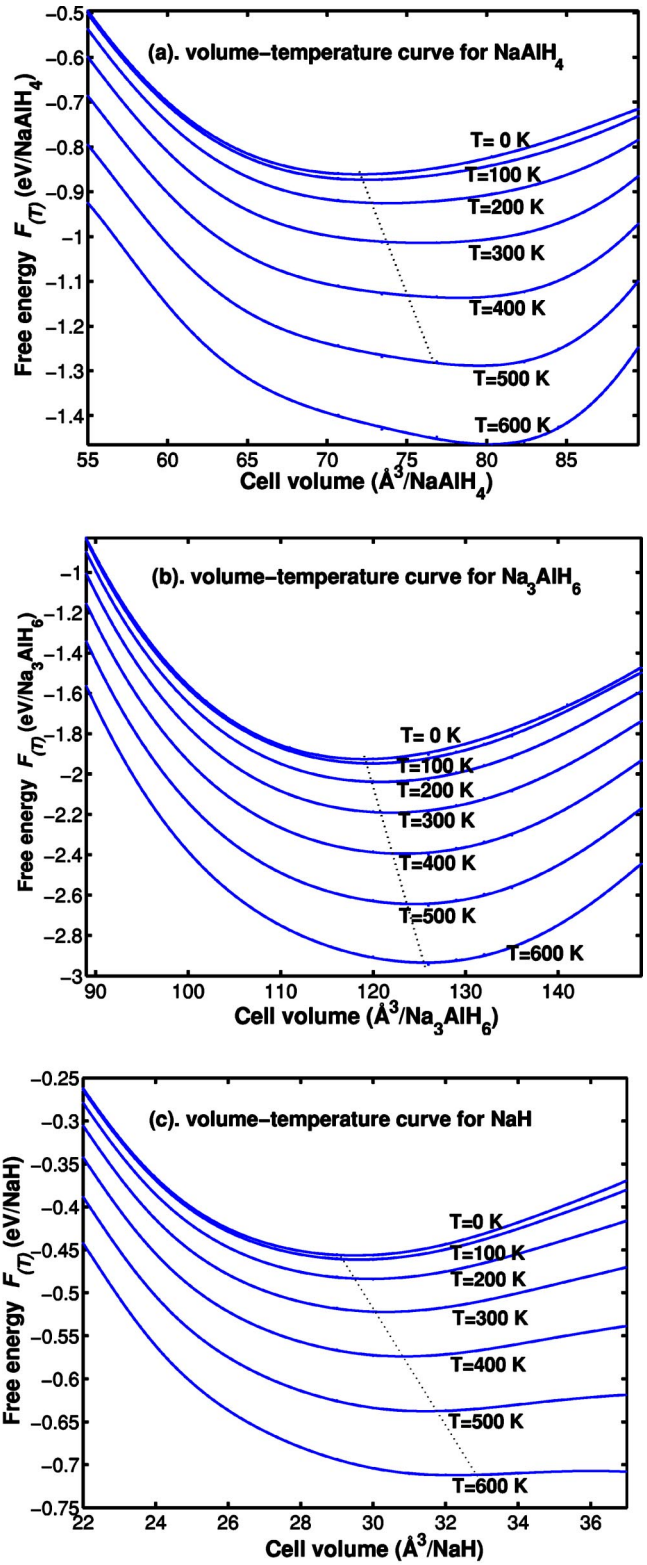


FIG. 7. Calculated Helmholtz free energy $F_{(T)}$ as a function of cell volume for $NaAlH_4$ [in (a)], $Na_3AlH_6$ [in (b)], and NaH [in (c)] in the temperature range from 0 to 600 K. Dotted lines connect the energy minima at different temperatures. The energies are calculated with respect to the elements in their standard states. (Here, for a fcc Al lattice, $E_{tot}=-3.705$ eV/atom. For a bcc Na lattice, $E_{tot}=-1.308$ eV/atom. For a $H_2$ molecule, $E_{tot}=-6.781$ eV per $H_2$.)

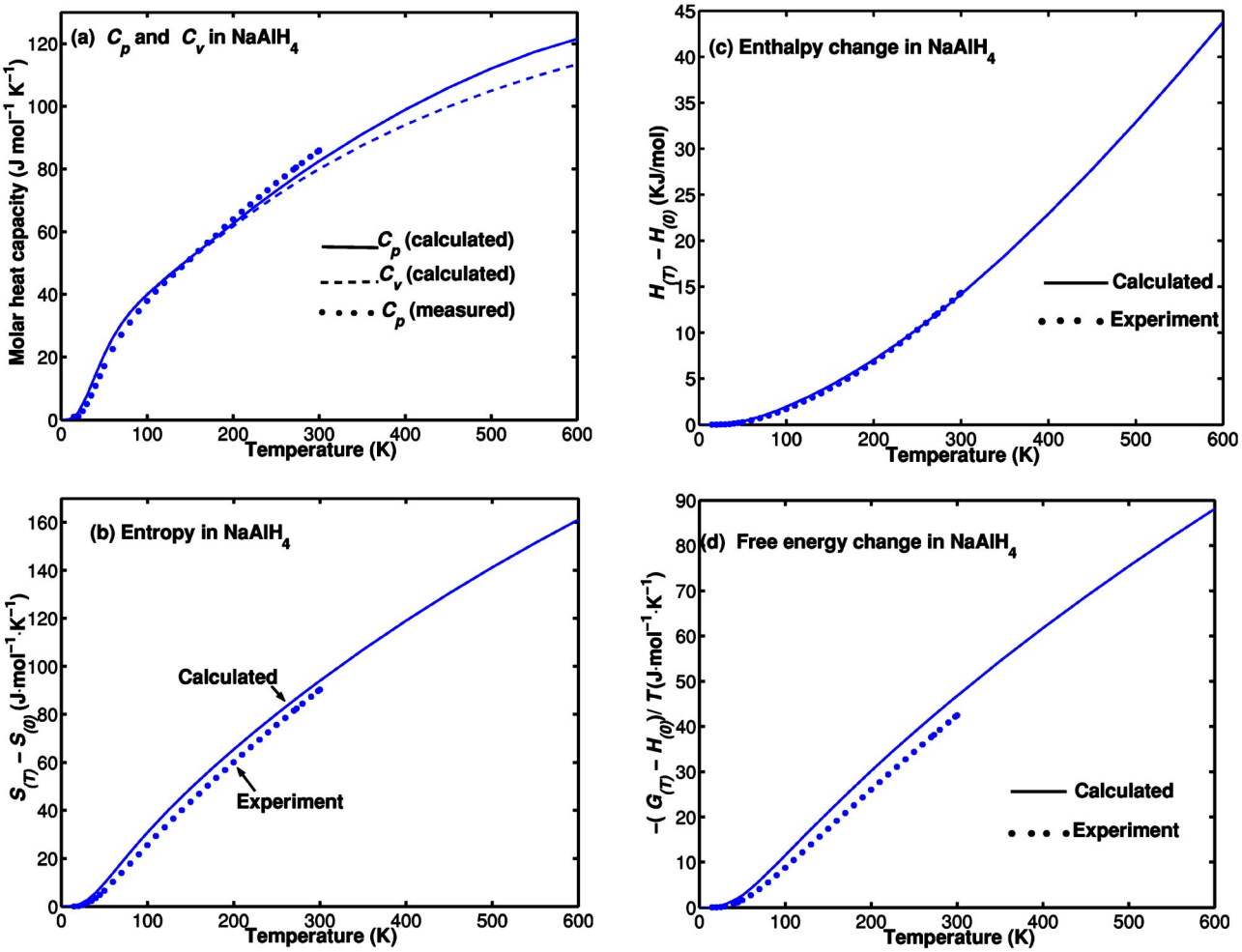


FIG. 8. Calculated and measured thermodynamic functions of $NaAlH_4$ (space group $I4_1/a$) as a function of temperature. The functions include the molar heat capacities of $C_p$ and $C_v$, the entropy of $S_{(T)}-S_{(0)}$, the vibrational enthalpy of $H_{(T)}-H_{(0)}$, and the free energy of $(G_{(T)}-H_{(0)})/T$. The symbols of $S_{(0)}$ and $H_{(0)}$ mean that the entropy and the enthalpy at 0 K, respectively. The measured data (in Ref. 5) are available in the temperature range from 10 to 300 K. Units here are K(J)/mol.

$$E_{(T)} = \frac{1}{2} r \int_0^\infty \hbar\omega g(\omega) \coth\left(\frac{\hbar\omega}{2k_B T}\right) d\omega. \tag{13}$$

In the low temperature limit the internal energy is equal to the ZP energy,

$$E_{zp} = \lim_{T\to 0} E_{(T)} = \frac{1}{2} r \int_0^\infty \hbar\omega g(\omega) d\omega. \tag{14}$$

Using these thermodynamic functions, we can obtain the enthalpy ($H_{(T)}$), the Helmholtz free energy ($F_{(T)}$), and the Gibbs free energy ($G_{(T)}$) of the unit cell,

$$H_{(T)} = E_{\text{elec}} + E_{(T)} + pV, \tag{15}$$

$$F_{(T)} = E_{\text{elec}} + E_{(T)} - TS_{(T)}, \tag{16}$$

$$G_{(T)} = H_{(T)} - TS_{(T)}, \tag{17}$$

where $E_{\text{elec}}$ is the electronic energy of the unit cell obtained from the first-principles total-energy calculations, and $p$ is the pressure. For solid-state materials at the standard pressure of 1 atm, usually the value of $pV$ term is quite small, e.g., $pV = 4.6\times10^{-5}$ eV for $NaAlH_4$ at 300 K, which is negligibly small.

To obtain the above thermodynamic functions, in practice, we use the quasiharmonic approximation (QHA), i.e., the phonons are harmonic, but they are volume dependent. In detail, the lattice volumes are expanded or compressed in our calculations. For each volume, the cell shape and the atomic coordinates are fully optimized until the forces are less than 0.0001 eV/Å (during the optimizations, the space-group symmetries for these materials were observed to be unchanged). After that, the phonons as well as the free energy $F_{(T)}$ are computed. The equilibrium volume at the temperature $T$ can be obtained by minimizing the free energy. The calculated volume-temperature curves for $NaAlH_4$, $Na_3AlH_6$, and NaH in the temperature range from 0 to 600 K are shown in Figs. 7(a)–7(c), respectively. For $NaAlH_4$, Fig. 7(a) shows that the curves look strange as the temperature $T \geqslant 500$ K. This may be due to the low melting point for $NaAlH_4$ [only 453 K (Ref. 6)]. Usually, the QHA is not valid

TABLE VII. Temperature-dependent volume, bulk moduli $B_0$, and thermal expansivity $\alpha[=(1/V)(\partial V/\partial T)]$ for $NaAlH_4$, $Na_3AlH_6$, and NaH in the temperature range from 0 to 600 K. The volume and bulk moduli are obtained by fitting the free energy curves (in Fig. 7) to the third order Birch-Murnaghan equation of state.

| Temperature (K) | 0 K | 100 K | 200 K | 300 K | 400 K | 500 K | 600 K |
|---|---|---|---|---|---|---|---|
| | | | $NaAlH_4$ | | | | |
| Equilibrium volume (Å$^3$) | 72.1 | 72.6 | 73.4 | 74.5 | 75.9 | 77.6*[a] | 79.6* |
| Bulk moduli $B_0$ (GPa) | 19.2 | 17.6 | 14.2 | 12.0 | 9.5 | 7.0* | 4.5* |
| Thermal expansivity $\alpha(\times 10^{-4}/\mathrm{K})$ | 0.0 | 0.42 | 0.83 | 1.25 | 1.66 | 2.08* | 2.50* |
| | | | $Na_3AlH_6$ | | | | |
| Equilibrium volume (Å$^3$) | 118.9 | 119.3 | 120.2 | 121.4 | 122.7 | 124.1 | 125.5 |
| Bulk moduli $B_0$ (GPa) | 29.6 | 28.8 | 27.4 | 26.2 | 25.1 | 24.3 | 23.9 |
| Thermal expansivity $\alpha(\times 10^{-4}/\mathrm{K})$ | 0.0 | 0.53 | 0.85 | 1.02 | 1.09 | 1.12 | 1.15 |
| | | | NaH | | | | |
| Equilibrium volume (Å$^3$) | 29.2 | 29.4 | 29.8 | 30.4 | 31.2 | 32.0 | 33.0 |
| Bulk moduli $B_0$ (GPa) | 23.4 | 23.2 | 22.2 | 21.0 | 19.5 | 17.5 | 14.8 |
| Thermal expansivity $\alpha(\times 10^{-4}/\mathrm{K})$ | 0.0 | 0.95 | 1.67 | 2.21 | 2.64 | 3.01 | 3.39 |

[a]The symbols of $*$ indicate that these values are less reliable because the free energy curves above the temperature 400 K in Fig. 7(a) are not suitable for the fitting of the Birch-Murnaghan equation of state.

any more as the temperature is close to the melting point of lattice.[37]

By fitting the free energy curves (in Fig. 7) to the third order Birch-Murnaghan equation of state,[38] we can obtain the temperature-dependent equilibrium volume, bulk moduli $B_0$, and thermal expansivity $\alpha$ $[=(1/V)(\partial V/\partial T)]$, which are compiled in Table VII. Table VII shows that these materials have low bulk moduli, indicating that they are quite soft, and can be easily compressed. It can be seen from the table that NaH has the largest thermal expansivity among these materials (although they have the same magnitude).

For $NaAlH_4$, the calculated and measured thermodynamic functions as a function of temperature are presented in Fig. 8. The functions include the molar heat capacities at the constant pressure ($C_p$) and at the constant volume ($C_v$), the entropy of $S_{(T)}-S_{(0)}$, the enthalpy of $H_{(T)}-H_{(0)}$, and the free energy of $(G_{(T)}-H_{(0)})T$. The symbols of $S_{(0)}$ and $H_{(0)}$ correspond to the entropy and the enthalpy at 0 K, respectively. The experimental data are available in the temperature range from 10 and 300 K.[5] Figure 8 shows that all of the calculated thermodynamic functions are in good agreement with the corresponding experimental data. This indicates that the QHA is valid for this lattice in this temperature range (0–300 K). It is noted that the melting point of $NaAlH_4$ is quite low (only 453 K).[6] As discussed in the preceding section, the QHA may be not valid as the temperature is close to the melting point. Thus the calculated thermodynamic functions may be less reliable as the temperature is close to 453 K.

For $Na_3AlH_6$, the calculated and measured thermodynamic functions as a function of temperature are presented in Fig. 9. The functions also include the molar heat capacities of $C_p$ and $C_v$, the entropy of $S_{(T)}-S_{(0)}$, the enthalpy of $H_{(T)}-H_{(0)}$, and the free energy of $(G_{(T)}-H_{(0)})/T$. The symbols of $S_{(0)}$ and $H_{(0)}$ also mean that the entropy and the enthalpy at 0 K, respectively. The measured data are available in the temperature range from 10 and 300 K.[5] Figure 9 shows that all of the calculated thermodynamic functions are in good agreement with the corresponding experimental data, indicating that the QHA is also valid for this lattice in the temperature range of our interest.

To make sure that the QHA also is valid for the lattice of NaH (space group, $Fm$-3$m$), we compare the calculated entropy of NaH with the experimental result, which is presented in Fig. 10. Figure 10 shows that the calculated result is in good agreement with the experimental data.

### D. Three decomposition reactions for $NaAlH_4$, $Na_3AlH_6$, and NaH

In the preceding section, it shows that all of the calculated thermodynamic functions of the lattices are in good agreement with experimental values. In this section, these functions are used to study the chemical reactions in Eqs. (1) and (2).

In order to study these chemical reactions, one needs to know the Gibbs free energy of a $H_2$ gas molecule at the standard pressure of 1 atm. For a gas molecule, the vibrations cannot be treated directly from the phonon calculations because the phonon approach always considers the system as a solid, and thus neglects the translational and rotational vibrational modes. The Gibbs free energy of a $H_2$ gas molecule is calculated by

$$G_{(T)}(\mathrm{H_2}) = E_{\mathrm{elec}}(\mathrm{H_2}) + E_{zp}(\mathrm{H_2}) + pV + \Delta G_{(T)}(\mathrm{H_2}), \quad (18)$$

where $E_{\mathrm{elec}}(\mathrm{H_2})$ is the electronic energy of a $H_2$ molecule obtained from the total-energy calculations, $E_{zp}(\mathrm{H_2})$ is the zero-point energy of a $H_2$ molecule obtained from the phonon calculations, $p$ and $V$ are the pressure (1 atm) and the molar volume (of the $H_2$ ideal gas), respectively, and the last term $\Delta G_{(T)}(\mathrm{H_2})$ is the temperature-dependent Gibbs free energy with respect to the temperature of 0 K. As a common

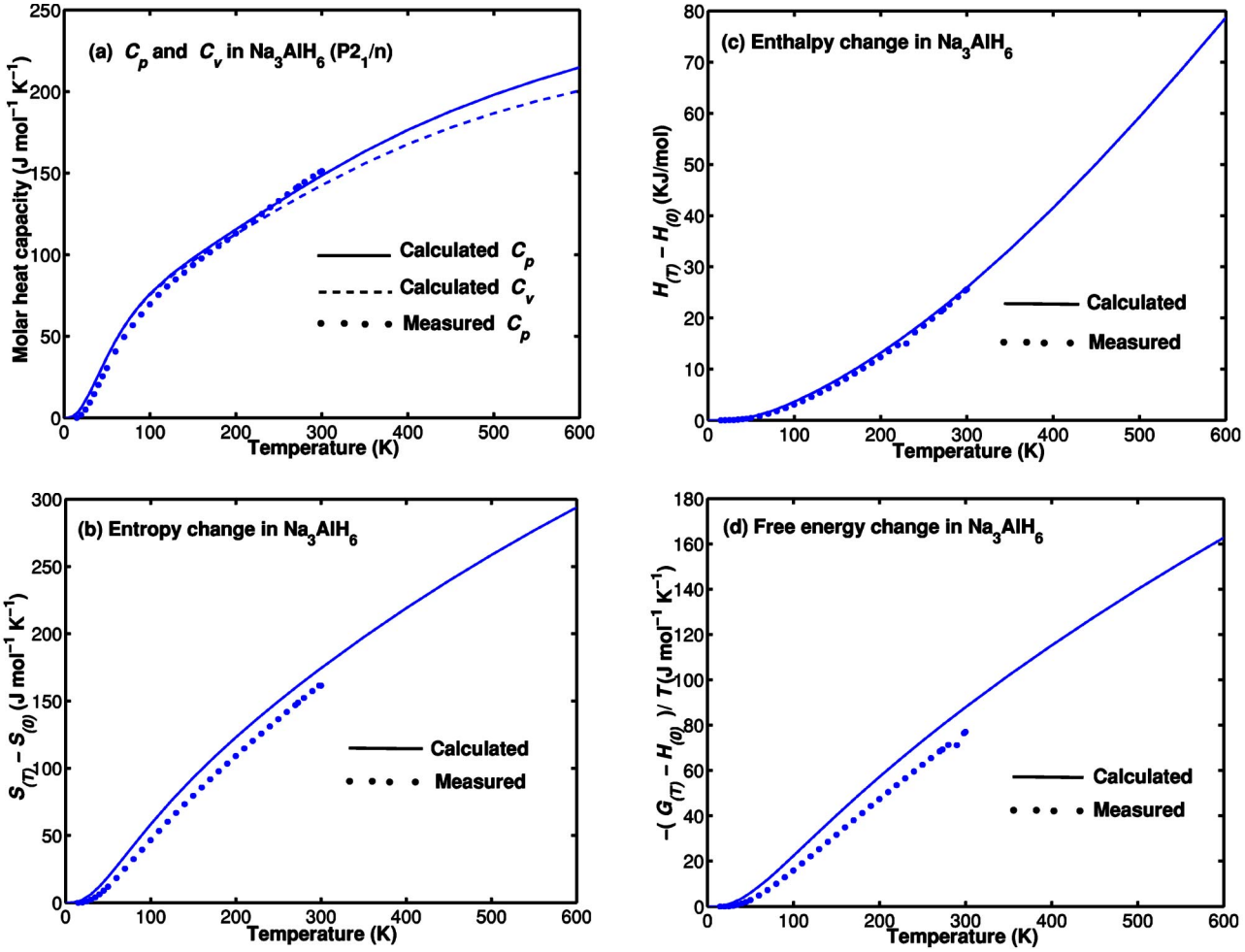


FIG. 9. Calculated and measured thermodynamic functions of $Na_3AlH_6$ (space group $P2_1/n$) as a function of temperature. The functions include the molar heat capacities of $C_p$ and $C_v$, the entropy of $S_{(T)}-S_{(0)}$, the enthalpy of $H_{(T)}-H_{(0)}$, and the free energy of $(G_{(T)}-H_{(0)})/T$. The symbols of $S_{(0)}$ and $H_{(0)}$ mean that the entropy and the enthalpy at 0 K, respectively. $S_{(0)}=0$. The measured data (in Ref. 5) are available in the temperature range from 10 to 300 K. Units are K(J)/mol.

procedure,[39] the $\Delta G_{(T)}(H_2)$ can be calculated by

$$\Delta G_{(T)}(H_2) = [H_{(T)}(H_2) - H_{(0)}(H_2)] - T \times [S_{(T)}(H_2) - S_{(0)}(H_2)], \quad (19)$$

where $H_{(T)}(H_2)$ and $H_{(0)}(H_2)$ are the enthalpies of the $H_2$ at the $T$ and 0 K, respectively, and $S_{(T)}(H_2)$ and $S_{(0)}(H_2)$ are the entropies of the $H_2$ at the $T$ and 0 K, respectively. Inputting the thermochemical data[41] to Eq. (19), we can obtain the values of $\Delta G_{(T)}(H_2)$, which are compiled in Table VIII.

For the fcc Al lattice, its free energy is calculated by the same procedure as that of the $H_2$,

$$G_{(T)}(Al) = E_{elec}(Al) + E_{zp}(Al) + \Delta G_{(T)}(Al), \quad (20)$$

where $E_{elec}(Al)$ (electronic energy), and $E_{zp}(Al)$ (zero-point energy) are obtained from the total-energy, and phonon calculations, respectively. $\Delta G_{(T)}(Al)$ is the temperature-dependent Gibbs free energy with respect to the temperature of 0 K, which can be obtained from the tabulated data.[40]

To study the reaction in Eq. (1), one needs to calculate the temperature-dependent Gibbs free energy difference ($\Delta G$) between $NaAlH_4$ and a sum of $(\frac{1}{3}Na_3AlH_6+\frac{2}{3}Al+H_2)$. For convenience, we denote $a=NaAlH_4$ and $b=(\frac{1}{3}Na_3AlH_6+\frac{2}{3}Al+H_2)$. The symbol of $\Delta G_{b-a}$ indicates that the Gibbs free energy difference between the $a$ and the $b$, i.e., $\Delta G_{b-a}=G_b-G_a$. A positive value of $\Delta G_{b-a}$ means that the $a$ is more stable than the $b$, a negative value of $\Delta G_{b-a}$ means that the $a$ is less stable than the $b$, and a zero value of $\Delta G_{b-a}$ means that the phase transition (or the chemical reaction) is just going to occur. The calculated Gibbs free energy difference of $\Delta G_{b-a}$ is plotted as a solid line in Fig. 11. The dotted line is the free energy of $NaAlH_4$, which is chosen as the zero reference. Figure 11 shows that the reaction is predicted to take place at the temperature of 285 K, which is in agreement with the recent experimental value of 353 K.[9] Given 1 eV≈11 600 K, then the error of 73 K is equivalent to 6 meV. This is rather small and therefore our predication is good. As discussed in the preceding section, the thermodynamic functions of $NaAlH_4$ may be less reliable as the temperature is close to the melting point of 453 K because of the

TABLE VIII. Temperature-dependent Gibbs free energy of $\Delta G_{(T)}(H_2)$ for a $H_2$ gas molecule with respect to the temperature of 0 K. $\Delta G_{(T)}(H_2)$ is obtained from Eq. (19), in which the enthalpy and entropy are taken from the thermochemical table at the pressure of 1 atm (in Ref. 41). In the experiment, the value of $H_{(298)}(H_2)$ is unknown (as a reference energy). Temperature-dependent entropy contributions of the $TS_{(T)}$ term for a $H_2$ gas molecule are also listed in the table, where the $S_{(T)}$ represents the absolute entropy of the $H_2$ at the temperature of $T$ (omitting contribution from nuclear spin). For an ideal gas, the hydrogen atom chemical potential of $\Delta\mu_{(T)}(H)=\frac{1}{2}\Delta G_{(T)}(H_2)$. Units are in eV.

| $T$ | $TS_{(T)}(H_2)$ | $\Delta G_{(T)}(H_2)$ | $T$ | $TS_{(T)}(H_2)$ | $\Delta G_{(T)}(H_2)$ |
|---|---|---|---|---|---|
| 100 K | 0.1058 eV | −0.0728 eV | 600 K | 0.9388 eV | −0.7597 eV |
| 200 K | 0.2473 eV | −0.1882 eV | 700 K | 1.1281 eV | −0.9186 eV |
| 300 K | 0.4066 eV | −0.3182 eV | 800 K | 1.3220 eV | −1.0818 eV |
| 400 K | 0.5767 eV | −0.4582 eV | 900 K | 1.5200 eV | −1.2489 eV |
| 500 K | 0.7547 eV | −0.6059 eV | 1000 K | 1.7216 eV | −1.4194 eV |

invalid QHA.[37] Therefore the free energy of $NaAlH_4$ may be less reliable as the temperature is close to 453 K. Thus the discussion of this reaction is mainly focused on the temperature range from 0 and 400 K. Note that this problem should not affect the predicted transition temperature of 285 K because in the preceding section we have shown that all of the calculated thermodynamic functions for $NaAlH_4$ are in good agreement with the experiment in the temperature range from 10 to 300 K. To check the individual contributions to the free energy, in Fig. 11 the enthalpy difference of $\Delta H_{b-a}$ and the entropy contribution difference of $T\Delta S_{b-a}$ are plotted as dots and a dashed line, respectively. The values of $\Delta H_{b-a}$ are almost constant (and positive) in the whole temperature range, indicating that this reaction are endothermic. At the $T=353$ K, the calculated value of $\Delta H_{b-a}$ at the pressure of 1 atm is 0.312 eV, which is in good agreement with the experimental value of 0.383 eV at 7 atm.[7] It can seen from the figure that the values of $T\Delta S_{b-a}$ are always positive, indicating that the entropy contribution in the $b$ is always larger than that in the $a$ (as the $T>0$ K). Therefore it can be concluded that the entropy contribution is the essential reason for the reaction to take place. The entropy contribution of $T\Delta S_{H_2}$ for a $H_2$ gas molecule is plotted as a dashed-dotted line in Fig. 11. It shows that the $T\Delta S_{H_2}$ is almost equal to the $T\Delta S_{b-a}$ as the $T<100$ K, and the $T\Delta S_{H_2}$ is slightly larger than the $T\Delta S_{b-a}$ as the $100\ \text{K}\leqslant T<300$ K. This indicates that the net entropy contribution to the reaction is approximately equal to the entropy contribution of a $H_2$ gas molecule. This also indicates that the entropy contributions from the solids are almost zero as the $T<100$ K, and are negative as the $T\geqslant 100$ K.

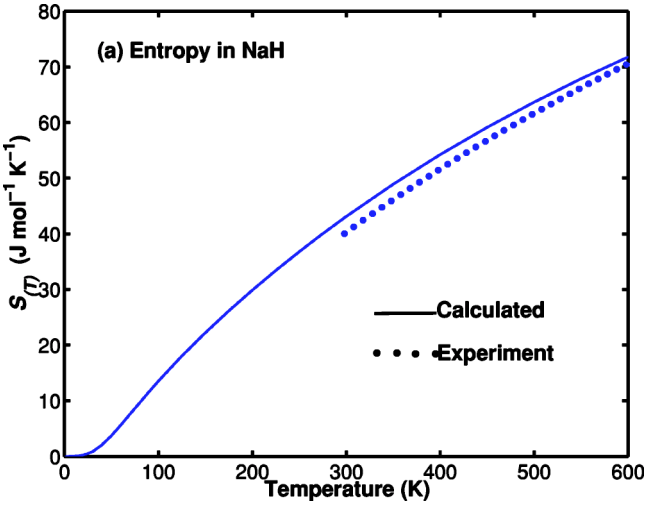


FIG. 10. Calculated and measured entropies of NaH lattice as a function of temperature. Experimental data for NaH are available from the temperature above 298 K (in Ref. 41). The units here are J mol$^{-1}$ K$^{-1}$. 1 J mol$^{-1}$=0.010 364 meV.

To study the reaction in Eq. (2), also for convenience, we denote $c=\frac{1}{3}Na_3AlH_6$ and $d=(NaH+\frac{1}{3}Al+\frac{1}{2}H_2)$. The symbol of $\Delta G_{d-c}$ indicates that the Gibbs free energy difference between the $c$ and the $d$, i.e., $\Delta G_{d-c}=G_d-G_c$. The temperature-dependent Gibbs free energy difference of $\Delta G_{d-c}$ is plotted as a solid line in Fig. 12. The free energy of $Na_3AlH_6$ is chosen as the zero reference (denoted as a dotted line). Figure 12 shows that the calculated transition temperature for the reaction is 390 K, which is in good agreement with the experimental value of 423 K.[6] To check the individual contributions to the reaction, the enthalpy difference of $\Delta H_{d-c}$ (denoted as dots) and the entropy contribution difference of $T\Delta S_{d-c}$ (denoted as a dashed line) are presented in Fig. 12. The values of $\Delta H_{b-a}$ are almost constant (and positive) in the whole temperature range, indicating that this reaction are endothermic. At the $T=500$ K, the calculated value of $\Delta H_{b-a}$ at the pressure of 1 atm is 0.275 eV, which is in agreement with the experimental value of 0.162 eV.[4] Similar to the first reaction, the entropy contribution also is the essential reason for this reaction to take place. The entropy contribution of $\frac{1}{2}T\Delta S_{H_2}$ for the $\frac{1}{2}H_2$ molecule is plotted as a dashed-dotted line in Fig. 12. It shows that the $\frac{1}{2}T\Delta S_{H_2}$ is almost equal to the $T\Delta S_{d-c}$ as the $T<200$ K, and the $\frac{1}{2}T\Delta S_{H_2}$ is slightly larger than the $T\Delta S_{d-c}$ in the temperature range from 200 to 400 K. This indicates that the net entropy contribution to the reaction is approximately equal to the entropy contribution of $\frac{1}{2}H_2$ gas molecule. This also indicates that the entropy contributions from the solids are almost zero as the $T<200$ K, and are negative as the $T\geqslant 200$ K.

After the second reaction [in Eq. (2)], only NaH contains hydrogen. It is interesting to study the decomposition of NaH. The reaction is as follows:

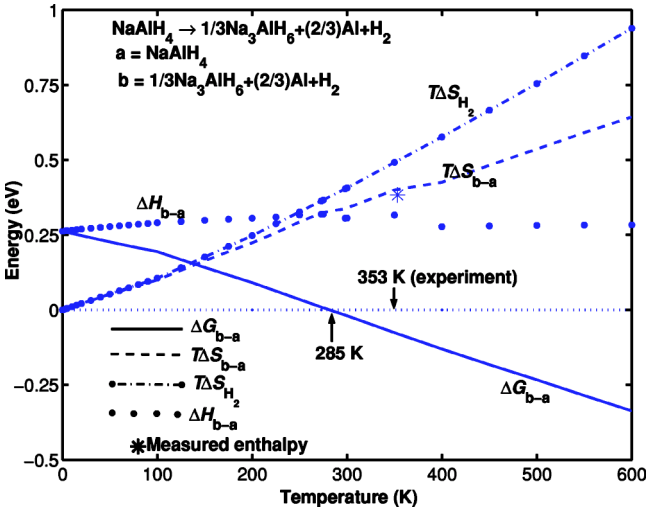


FIG. 11. Temperature-dependent energy differences between $NaAlH_4$ and a sum of $(\frac{1}{3}Na_3AlH_6+\frac{2}{3}Al+H_2)$. For convenience, we suppose $a=NaAlH_4$ and $b=(\frac{1}{3}Na_3AlH_6+\frac{2}{3}Al+H_2)$. Symbol of $\Delta G_{b-a}$ indicates that the Gibbs free energy difference between the $a$ and the $b$, i.e., $\Delta G_{b-a}=G_b-G_a$. The energy differences include the Gibbs free energy difference of $\Delta G_{b-a}$ (denoted as a solid line), the entropy contribution difference of $T\Delta S_{b-a}$ (as a dashed line), and the enthalpy difference of $\Delta H_{b-a}$ (as dots). The entropy contribution of $T\Delta S_{H_2}$ for a $H_2$ molecule is plotted as a dashed-dotted line. The energies of $NaAlH_4$ are always chosen as the zero reference (as a dotted line). The mark of $*$ represents the measured enthalpy (0.383 eV) of $\Delta H_{b-a}$ (in Ref. 7). These curves may be less reliable as the temperature is close to 453 K (see the text for detail).

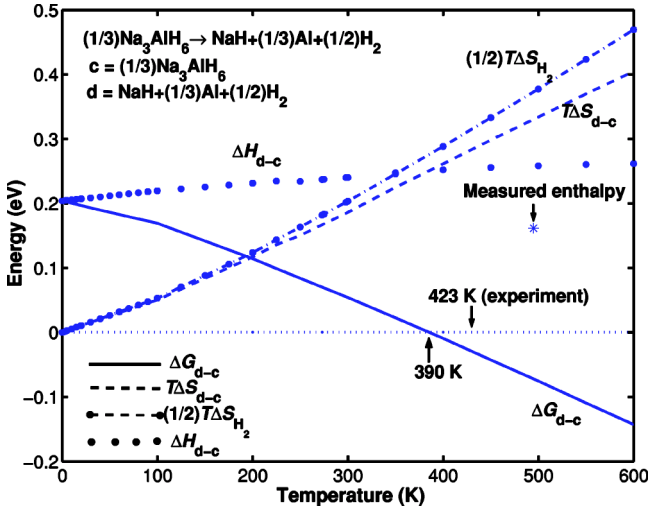


FIG. 12. Temperature-dependent energy differences between $(\frac{1}{3}Na_3AlH_6)$ and a sum of $(NaH+\frac{1}{3}Al+\frac{1}{2}H_2)$. For convenience, we denote $c=\frac{1}{3}Na_3AlH_6$ and $d=(NaH+\frac{1}{3}Al+\frac{1}{2}H_2)$. Symbol of $\Delta G_{d-c}$ indicates that the Gibbs free energy difference between the $c$ and the $d$, i.e., $\Delta G_{d-c}=G_d-G_c$. The energy differences include the Gibbs free energy difference of $\Delta G_{d-c}$ (denoted as a solid line), the entropy contribution difference of $T\Delta S_{d-c}$ (denoted as a dashed line), and the enthalpy difference of $\Delta H_{d-c}$ (denoted as dots). The entropy contribution of $\frac{1}{2}T\Delta S_{H_2}$ for $\frac{1}{2}H_2$ molecules is plotted as a dashed-dotted line. The energies of $Na_3AlH_6$ are always chosen as the zero reference (denoted as a dotted line). The calculated and measured (in Ref. 6) transition temperatures for this reaction are 390 and 423 K, respectively.

$$NaH \xrightarrow{698\ K} Na+\tfrac{1}{2}H_2, \quad \Delta H=0.591\ eV, \qquad (21)$$

where 698 K is the experimental transition temperature for this reaction and $\Delta H=0.591$ eV is the experimental reaction enthalpy.[42] To study this reaction, one needs to be careful in the sodium structure because the melting point of the Na lattice is quite low (only 371 K), and the QHA may not be valid as the temperature is close to the melting point.[37] In the temperature range from 298 to 1170 K, the thermodynamic functions for both the solid and liquid sodium can be obtained from the thermochemical table.[41] For the temperature $T<298$ K, the thermodynamic functions of the solid were calculated on the basis of the QHA. To study this reaction, also for convenience, we denote $e=NaH$ and $f=Na+\frac{1}{2}H_2$. We have also calculated the Gibbs free energy difference ($\Delta G_{f-e}$), the enthalpy difference ($\Delta H_{f-e}$) and the entropy contribution difference ($T\Delta S_{f-e}$) between the $e$ and the $f$ (not plotted). The calculated results show that the reaction is predicted to take place at 726 K, which is in good agreement with the experimental value of 698 K. The calculated value of $\Delta H_{f-e}$ is equal to 0.48 eV at the $T=0$ K, and the values vary from 0.48 to 0.54 eV as the $T>0$ K, which are in agreement with the experimental value of 0.59 eV. The calculations also confirm that the entropy contribution is the essential reason for the reaction to take place. The calculated results also indicate that the net entropy contribution to the reaction is approximately equal to the entropy contribution of $\frac{1}{2}H_2$ gas molecule.

## IV. CONCLUDING REMARKS

The electronic properties and lattice dynamics of the sodium alanate phases have been studied by the first-principles method. The phases include $NaAlH_4$, $Na_3AlH_6$, and NaH. The space groups for $NaAlH_4$, $Na_3AlH_6$, and NaH are $I4_1/a$, $P2_1/n$, and $Fm$-$3m$, respectively.

The electronic properties of the phases are discussed on the basis of the electronic band structures, the atomic charges, the bond overlap population analysis, and the Born effective charge tensors. The following points have been demonstrated:

(i) The calculated band gaps for $NaAlH_4$, $Na_3AlH_6$, and NaH are 4.8, 2.7, and 4.9 eV, respectively, indicating these lattices are strongly ionic crystals. The electronic band dispersion relations of $Na_3AlH_6$ are somewhat similar to those of $NaAlH_4$, e.g., the minimum direct band gaps for both lattices are located at the $\Gamma$ point, and the dispersion relations at the highest occupied states (more or less at the lowest unoccupied states) are similar for both lattices. This indicates that the lattices of $NaAlH_4$ and $Na_3AlH_6$ belong to the same class of crystals.

(ii) Based on the Mulliken charge analysis, the total charge of a H atom in these lattices is larger than 1.0 electron. This situation is similar to that of H in metals, where the H atom always accepts electrons from metals (in particular for transition metals). However, this does not mean these lattices are metals. The partial DOS shows that the H band in

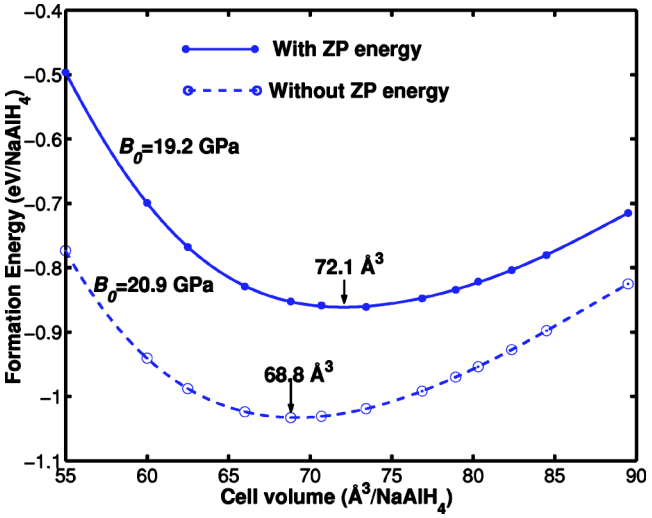


FIG. 13. Calculated formation energy of $NaAlH_4$ as a function of cell volume at the temperature $T=0$ K. The dashed line represents the results without considering the zero-point energy. The solid line represents the results including the zero-point energy. The formation energy is calculated with respect to the element in the standard state. The bulk moduli with and without the ZP energy are also given.

the lattices is very different from that of H in metals. For H in these lattices, the whole valence bands are strongly dominated by the H atom. While for H in metals (except alkali metals), the main position of the H band usually is below the valence band of the host metals (relative to the Fermi level).

(iii) The bond overlap population analysis indicates that the H—Al bonds are covalent, and the covalent H—Al bonds in $NaAlH_4$ are stronger than those in $Na_3AlH_6$. On the other hand, the H—Na bonds are ionic. The interactions between the H—H atoms are found to be very weak.

(iv) The values of the dynamics charges in the lattices are close to the nominal ionic charges (+1 for Na and −1 for H) except for the Al atom. For the Al atom, its dynamics charges are 1.64–2.08, which are smaller than the nominal charge of +3.

The phonon dispersion relations and phonon density of states of the lattices are calculated by using a direct force-constant method. The phonons are harmonic. The following points have been demonstrated:

(i) Since the mass of H atom is much smaller than that of Na or Al atom, the high frequency modes in the lattices are dominated by H atom, and the low frequency modes are dominated by Na and Al atoms. For $NaAlH_4$ and $Na_3AlH_6$, Al atoms participate in the high frequency modes due to the vibrational coupling between the H and Al atoms. For NaH, the high frequency modes of H atom are almost completely separated from the low frequency modes of Na atom.

(ii) The calculated Raman frequencies of $NaAlH_4$ are in good agreement with experimental values within 5% error.

(iii) For H vibrations in $NaAlH_4$, there is a big gap between the high and low frequency modes (of H atom). While for H vibrations in $Na_3AlH_6$, there is not such a big gap. Qualitatively, this difference can be understood in terms of the bond overlap population analysis.

(iv) For NaH, there is a giant LO/TO splitting between $T_{1u}$(TO) and $T_{1u}$(LO) modes at the $\Gamma$ point. While for $NaAlH_4$ and $Na_3AlH_6$, the LO/TO splittings are not significant.

The thermodynamic functions are obtained from the integrated phonon DOS within the quasiharmonic approximation. The functions include the heat capacity ($C_v$ and $C_p$), the vibrational enthalpy ($H_{(T)}$), the entropy ($S_{(T)}$), and the Gibbs free energy. All of the calculated thermodynamic functions of the lattices are in good agreement with experimental values.

Three decomposition reactions are studied on the basis of the thermodynamic functions. The reactions include (1) $NaAlH_4 \rightarrow \frac{1}{3}Na_3AlH_6 + \frac{2}{3}Al + H_2$, (2) $\frac{1}{3}Na_3AlH_6 \rightarrow NaH + \frac{1}{3}Al + \frac{1}{2}H_2$, and (3) $NaH \rightarrow Na + \frac{1}{2}H_2$. The following points have been obtained:

(i) The reactions (1), (2), and (3) are predicted to take place at 285 K, 390 K, and 726 K, respectively, which are in good agreement with the experimental values (353 K, 423 K, and 698 K, respectively). The errors in our case are within 100 K.

(ii) The calculated values of the enthalpies for the reactions are almost constant, and positive in the whole temperature range. This means that the reactions are endothermic. The calculations confirm that the entropy contribution is the essential reason for the reactions to take place.

(iii) Concerning the entropy contribution ($T\Delta S$) to the reactions, we found an interesting result, i.e., the net entropy contribution to the reaction is approximately equal to the entropy contribution of the $H_2$ gas molecule produced in that reaction. For the first reaction, the entropy contribution ($T\Delta S_{b-a}$) is approximately equal to that of a $H_2$ gas molecule ($T\Delta S_{H_2}$). For the second or third reaction, the entropy contribution ($T\Delta S_{d-c}$ or $T\Delta S_{f-e}$) is approximately equal to that of $\frac{1}{2}H_2$ gas molecule ($\frac{1}{2}T\Delta S_{H_2}$). It is interesting to see whether

TABLE IX. Calculated zero-point (ZP) energies for $NaAlH_4$ (space group $I4_1/a$), $Na_3AlH_6$ (space group $P2_1/n$), NaH (space group $Fm$-$3m$), and a $H_2$ dimer at their equilibrium positions.

| Units | $NaAlH_4$ | $Na_3AlH_6$ | NaH | $H_2$ |
|---|---|---|---|---|
| eV per formal cell (eV/f.u.) | 0.800 | 1.167 | 0.157 | 0.284 |
| eV per hydrogen atom (eV/H atom)[a] | 0.200 | 0.195 | 0.157 | 0.142 |

[a]The values are roughly estimated by omitting the contributions from the Na and Al atoms. In general, the ZP energy contributions from Na and Al atoms are quite small because the frequency modes for these two atoms are quite low. For example, the majority of the frequency region for the Al atom in $NaAlH_4$ is almost the same as that for the Al in the fcc Al lattice. For Al in the fcc lattice, the ZP energy is only 0.034 eV/atom.

TABLE X. Calculated reaction enthalpies with and without the zero-pint energies for the reactions in Eqs. (1), (2), and (21) at the temperature $T=0$ K.

| Reaction enthalpy | With the ZP energy | Without the ZP energy |
|---|---|---|
| $\Delta H_{b-a}$ in Eq. (1) | 0.23 eV | 0.32 eV |
| $\Delta H_{d-c}$ in Eq. (2) | 0.19 eV | 0.26 eV |
| $\Delta H_{f-e}$ in Eq. (21) | 0.46 eV | 0.45 eV |

this phenomenon can be applied to other reactions. Let us take another example, the reaction for the metastable $AlH_3$ (space group $R\bar{3}c$) is as follows:

$$AlH_3 = Al + \tfrac{3}{2}H_2. \quad (22)$$

The calculated heat capacities ($C_p$) of $AlH_3$ are in good agreement with the measured data[43] as well as the other calculated results[44] (not plotted here). This indicates that the QHA is valid for this material. Interestingly, the calculated results also show that the net entropy contribution to the reaction is approximately equal to the entropy contribution of the $\frac{3}{2}H_2$ gas molecule (not plotted). According to this rule, in principle, the transition temperature for this kind of reaction (product contains $H_2$ gas) can be roughly predicted if the reaction enthalpy at the $T=0$ is known. The enthalpy at the $T=0$ can be easily obtained from the total energy calculations, and the enthalpy can be roughly considered to be constant according to the above investigation. At the moment, this rule was found to be not valid if the reactant contains another very light element such as Li in $LiAlH_4$ (see Table V in Ref. 14).

Since these lattices contain hydrogen atoms, and the hydrogen mass is quite light, the quantum-mechanical effect (such as the zero-point energy) may play a certain role in the properties of the lattices. In the current study, the following points have been demonstrated:

(i) The calculated zero-point (ZP) energies for $NaAlH_4$, $Na_3AlH_6$, NaH, and a $H_2$ dimer are compiled in Table IX. Omitting the contributions from the Na and Al atoms, we can see that the ZP energies for the H atom in $NaAlH_4$ and $Na_3AlH_6$ are larger than that for the H in the $H_2$. This is understandable since the highly covalent H—Al bond leads to the high frequency modes for the H in these lattices. For the H atom in NaH, the ZP energy is almost the same as that in the $H_2$.

(ii) The ZP energy slightly expands the lattice constant. Figure 13 shows that the calculated formation energy of $NaAlH_4$ as a function of cell volume. The solid and dashed lines represent the results with and without considering the zero-point energy, respectively. It shows that the zero-point motion can slightly expand the lattice constant (also see Table II).

(iii) The ZP energy affects the formation energy. For $NaAlH_4$ at the equilibrium site, Fig. 13 shows that the formation energy difference with and without the ZP energy is 0.17 eV. For NaH, the ZP energy less affects the formation energy because the ZP energy in NaH is almost the same as that in the $H_2$ (see Table IX).

(iv) The ZP energy slightly affects the reaction enthalpy. The reaction enthalpies with and without the zero-point energies for the reactions in Eqs. (1), (2), and (21), at the $T=0$ K are compiled in Table X. For $NaAlH_4$ and $Na_3AlH_6$, Table X shows that the enthalpies with the ZP energy are slightly smaller than those without the ZP energy. Inversely, for NaH the enthalpy with the ZP energy is slightly larger than that without the ZP energy. The reason is that the H—Al bonds in $NaAlH_4$ and $Na_3AlH_6$ are much more covalent than the H—Na (ionic) bond in NaH, which causes larger ZP energies in $NaAlH_4$ and $Na_3AlH_6$ than that in NaH (also see Table IX for the ZP energies).

(v) The ZP energy slightly affects the shape of the potential energy well. Figure 13 shows that the bulk modulus decreases a bit if the zero-point energy is included.

In principle, it is possible to study the reactions under the condition of the doped catalyst in this way. In order to do that, above all, the exact sites of the doped atoms should be located. We can imagine that the computational demand for the doped system will be great because the symmetries including the point group and the space group will be partially or completely broken.

## ACKNOWLEDGMENTS

The authors thank Dr. M. Marsman and Dr. Lixin He for the help of Born effective charge calculations. The authors also thank Professor G. J. Kramer, Dr. A. Kuwabara, Dr. T. Yamamoto, Dr. W. Bergermayer, Dr. B. Yebka, Dr. C. M. Fang, and T. Tohei, and financial support of MEXT Japan on Computational Materials Science Unit in Kyoto University.

*Electronic address: ke@fukui.kyoto-u.ac.jp
†Electronic address: tanaka@cms.mt1.kyoto-u.ac.jp

[1] J. H. Hirschenhofer, D. B. Stauffer, and R. R. Engleman, *Fuel Cell Technology Handbook*, (CRC Press, Boca Raton, FL, 2003).
[2] B. Bogdanović and M. Schwickardi, J. Alloys Compd. **253**, 1 (1997).
[3] B. Bogdanović, R. A. Brand, A. Marjanović, M. Schwickardi, and J. Tölle, J. Alloys Compd. **302**, 36 (2000).
[4] P. Claudy, B. Bonnetot, G. Chahine, and J. M. Létoffé, Thermochim. Acta **38**, 75 (1980).
[5] B. Bonnetot, G. Chahine, P. Claudy, M. Diot, and J. M. Létoffé, J. Chem. Thermodyn. **12**, 249 (1980).
[6] K. J. Gross, S. Guthrie, S. Takara, and G. Thomas, J. Alloys Compd. **297**, 270 (2000).
[7] C. M. Jensen and K. J. Gross, Appl. Phys. A: Mater. Sci. Process.

**72**, 213 (2001).
[8] D. J. Ross, M. D. Halls, A. G. Nari, and R. F. Aroca, Chem. Phys. Lett. **388**, 430 (2004).
[9] B. Yebka and G. A. Nari, Mater. Res. Soc. Symp. Proc. **801**, 133 (2004).
[10] P. Vajeeston, P. Ravindran, R. Vidya, H. Fjellvåg, and A. Kjekshus, Appl. Phys. Lett. **82**, 2257 (2003).
[11] A. Aguayo and D. J. Singh, Phys. Rev. B **69**, 155103 (2004).
[12] S. M. Opalka and D. L. Anton, J. Alloys Compd. **356**, 486 (2003).
[13] M. E. Arroyo y de Dompablo and G. Ceder, J. Alloys Compd. **364**, 6 (2004).
[14] O. M. Løvvik, S. M. Opalka, H. W. Brinks, and B. C. Hauback, Phys. Rev. B **69**, 134117 (2004).
[15] G. Kresse and J. Furthmüller, Comput. Mater. Sci. **6**, 15 (1996).
[16] G. Kresse and J. Furthmüller, Phys. Rev. B **54**, 11 169 (1996).
[17] J. P. Perdew, J. A. Chevary, S. H. Vosko, K. A. Jackson, M. R. Pederson, D. J. Singh, and C. Fiolhais, Phys. Rev. B **46**, 6671 (1992).
[18] P. E. Blöchl, Phys. Rev. B **50**, 17 953 (1994).
[19] G. Kresse and D. Joubert, Phys. Rev. B **59**, 1758 (1999).
[20] H. J. Monkhorst and J. D. Pack, Phys. Rev. B **13**, 5188 (1976).
[21] K. Parlinski, Z. Q. Li, and Y. Kawazoe, Phys. Rev. Lett. **78**, 4063 (1997); **81**, 3298 (1998).
[22] K. Kunc and R. Martin, Phys. Rev. Lett. **48**, 406 (1982).
[23] A. J. Read and R. J. Needs, Phys. Rev. B **44**, 13071 (1991).
[24] R. M. Pick, M. H. Cohen, and R. M. Martin, Phys. Rev. B **1**, 910 (1970).
[25] X. Gonze, J. C. Charlier, D. C. Allan, and M. P. Teter, Phys. Rev. B **50**, 13 035 (1994).
[26] W. Zhong, R. D. King-Smith, and D. Vanderbilt, Phys. Rev. Lett. **72**, 3618 (1994).
[27] C. G. Shull, E. O. Wollan, G. A. Morton, and W. L. Davidson, Phys. Rev. **73**, 842 (1948).
[28] M. Radny, J. Phys.: Condens. Matter **3**, 5525 (1991).
[29] R. S. Mulliken, J. Chem. Phys. **23**, 1833 (1955).
[30] M. D. Segall, P. L. D. Lindan, M. J. Probert, C. J. Pickard, P. J. Hasnip, S. J. Clark, and M. C. Payne, J. Phys.: Condens. Matter **14**, 2717 (2002).
[31] E. R. Davidson and S. Chakravorty, Theor. Chim. Acta **83**, 319 (1992).
[32] M. D. Segall, R. Shah, C. J. Pickard, and M. C. Payne, Phys. Rev. B **54**, 16317 (1996).
[33] H. Smithson, C. A. Marianetti, D. Morgan, A. Van der Ven, A. Predith, and G. Ceder, Phys. Rev. B **66**, 144107 (2002).
[34] X. Z. Ke, G. J. Kramer, and O. M. Løvvik, J. Phys.: Condens. Matter **16**, 6267 (2004).
[35] R. Resta, Rev. Mod. Phys. **66**, 899 (1994).
[36] R. D. King-Smith and D. Vanderbilt, Phys. Rev. B **47**, 1651 (1993).
[37] S. Baroni, S. de Gironcoli, and A. D. Corso, Rev. Mod. Phys. **73**, 515 (2001).
[38] J. P. Poirier, *Introduction to the Physics of the Earth's Interior*, 2nd ed. (Cambridge University Press, New York, 2000).
[39] K. Reuter and M. Scheffler, Phys. Rev. B **65**, 035406 (2001).
[40] D. A. Ditmars, C. A. Plint, and R. C. Shukla, Int. J. Thermophys. **8**, 621 (1987).
[41] D. R. Stull and H. Prophet, *JANAF Thermochemical Tables*, 2nd ed. (U.S. National Bureau of Standards, Washington, DC, 1971).
[42] A. F. Hollemann and E. Wiberg, in *Lehrbuch der Anorgansichen Chemie* (Walter de Gruyter, Berlin, 1995), p. 1169. This reference (in German) was not found. The experimental data including the transition temperature (425 °C) and the reaction enthalpy (57 K J/mol) can be obtained indirectly from Ref. 3. Usually, the enthalpy is temperature dependent. But we do not know the experimental temperature for this enthalpy.
[43] G. C. Sinke, L. C. Walker, F. L. Oetting, and D. R. Stull, J. Chem. Phys. **47**, 2759 (1967).
[44] C. Wolverton, V. Ozoliņš, and M. D. Asta, Phys. Rev. B **69**, 144109 (2004).